Atmos. Chem. Phys. Discuss., 6, 5197–5229, 2006
www.atmos-chem-phys-discuss.net/6/5197/2006/

Atmospheric Chemistry and Physics Discussions

Regional lightning NO_x sources during the TROCCINOX experiment

C. Mari[1], J. P. Chaboureau[1], J. P. Pinty[1], J. Duron[1], P. Mascart[1], J. P. Cammas[1], F. Gheusi[1], T. Fehr[2], H. Schlager[2], A. Roiger[2], M. Lichtenstein[2], and P. Stock[2]

[1]Laboratoire d'Aérologie, UMR CNRS/UPS, Toulouse, France
[2]DLR, Institut fuer Physik der Atmosphaere, Oberpfaffenhofen, Wessling, Germany

Received: 8 February 2006 – Accepted: 28 February 2006 – Published: 26 June 2006

Correspondence to: C. Mari (celine.mari@aero.obs-mip.fr)

Abstract

A lightning NO_x source (LiNOx) has been implemented in the deep convection scheme of the Meso-NH mesoscale model following a mass-flux formalism coherent with the transport and scavenging of gases inside the convective scheme. No a-priori vertical placement of LiNOx is necessary with this approach. In this approach the vertical transport of NO inside clouds is calculated by the parameterization of deep convective transport, thus eliminating the need for a-priori LiNOx. Once produced inside the convective column, NO molecules are redistributed by updrafts and downdrafts and detrained in the environment when the conditions are favorable. The model was applied to three particular flights during the Tropical Convection, Cirrus and Nitrogen Oxides (TROCCINOX) campaign over the tropical area around Bauru on 3–4 March 2004. The convective activity during the three flights was investigated using brightness temperature at 10.7 μm observed from GOES-12 satellite. The use of a model-to-satellite approach reveals that the simulation appears rather realistic compared to the observations. The diurnal cycle of the simulated brightness temperature, CAPE, number of IC lightning, NO entrainment flux are in phase, with a succession of three marked peaks at 18:00 UTC (15:00 LT). These simulated peaks precede the observed afternoon one by about three hours. Comparison of the simulated NO_x with observations along the flight tracks show that the model reproduces well the observed NO_x levels when the LiNOx source is applied. The budget of entrainment, detrainment and LiNOx convective fluxes shows that the majority of the NO detrained back to the environment comes from lightning source inside the convective columns. Entrainment of NO from the environment and vertical transport from the boundary layer were not significant during the episode. The troposphere is impacted by detrainment fluxes of LiNOx from 4 km altitude to 16 km with maximum values around 14 km altitude. Detrainment fluxes vary between 75 kg(N)/s during nighttime to 400 kg(N)/s at the times of maximun convective activity. Extrapolation of these regional fluxes gives global LiNOx production between 39-55 Tg(N)/year which is above the upper range of current estimates.

1 Introduction

Ozone is produced in the troposphere by photochemical oxidation of hydrocarbons and CO catalysed by hydrogen oxide radicals (HO_x=OH+HO_2) and nitrogen oxide radicals (NO_x=NO+NO_2). Consequently changes in atmospheric NO_x concentrations can lead to a modification in the rate of ozone production. NO_x is emitted into the atmosphere from various natural and anthropogenic sources, including fossil fuel combustion, biomass burning, aircraft emission and lightning (Brasseur et al., 1996; Bradshaw et al., 2000). Evidences of NO_x production by lightning were given by airborne measurements in and near mature thunderstorms. Observations at different latitudes show that NO_x can be increased considerably (as much as a few ppbv) in the upper troposphere on small spatial scales Huntrieser et al., 1998; Dye et al., 2000; Huntrieser et al., 2002; Skamarock et al., 2003).

It is still poorly known how much NO_x is produced by the storms and how this production relates to cloud parameters like particle phase, updraft strength, cloud top height, or flash rate, which all would be useful for parameterisations of NO_x-production. Consequently, estimates of the global NO_x production by lightning (hereafter LiNOx) in thunderstorms still differ by about one order of magnitude, between 1–20 Tg(N)/year Price et al., 1997; Lee et al., 1997; Huntrieser et al., 1998). This uncertainty can have great implications in terms of NO_x budget, especially in the southern hemisphere where the LiNOx source dominates. (Lamarque et al., 1997; Zhang et al., 2000; Martin et al., 2000; Hauglustaine et al., 2001).

Although the convective clouds and lightning are local processes, the impact of LiNOx source is global. The typical lifetime of NO_x increases from a few hours in the planetary boundary layer to a few days in the upper troposphere, where it can recycle HNO_3 and PAN. LiNOx is closely linked with OH radical production and hence can impact on the oxidizing capacity of the troposphere (Labrador et al., 2004). The chemistry within the high NO_x plume originated from lightning, their long-range transport and their potential importance in sustaining background NO_x far from source regions is still a challenge for global and regional model (Crawford et al., 2000; Tie et al., 2001; Brunner et al., 2003; DeCaria et al., 2005).

Recent satellite observations have demonstrated that, on the global scale, lightning activity is highest over tropical continental areas (Christian et al., 2003). The Tropical Convection, Cirrus and Nitrogen Oxides (TROCCINOX) experiment took place over southern Brazil and provided the first measurements of LiNOx near deep convective clouds over a continental region in the tropics. This paper focuses on particular convective episodes of the TROCCINOX 2004 experiment when LiNOx production was found in the upper troposphere. The objective is to quantify the amounts of LiNOx produced in well-characterised cloud formations and scale up the results of the mission to provide regional estimates of lightning NO_x.

2 Model description

The model used in this study is the Meso-NH model. A full description of the model capabilities is available on http://www.aero.obs-mip.fr/mesonh (Lafore et al., 1998). One single domain is used with a horizontal grid of 100×100 points at 30 km resolution and 70 levels from 40 m (bottom) up to 600 m (top). The time step is 30 s. The model starts on 2 March at 00:00 UTC and runs for 66 h. The physics of the model includes the prognostic calculation of the turbulence and a convection scheme based on mass-flux calculations (Bechtold et al., 2001). A mixed-phase microphysics and the subgrid cloudiness are available for these simulations. The surface fluxes are provided by the ISBA (Interaction among Soil-Biosphere-Atmosphere) model (Noilhan, 1989) for the natural patches and TEB (Town Energy Balance) model (Masson et al., 2000) for the urbanized patches. The radiation scheme is the ECMWF scheme (Mlawer et al., 1997). The chemistry scheme includes 37 chemical species representative of the O3-NOx-VOC chemistry (Crassier et al., 2000). Emissions are from the EDGAR 3.2 1995 database (Olivier et al., 2001a, b).

The initial and large-scale mixing ratios for chemistry are provided by the MOCAGE

(MOdele de Chimie Atmospherique de Grande Echelle) model (Josse et al., 2004; Massart et al., 2005).

The deep convection scheme of Meso-NH (Kain and Fritsch, 1990; Bechtold et al., 2001) has been already adapted by Mari et al. (2000) for the transport and the scavenging of soluble gases.

The mass flux formalism applied to the convective transport of a chemical compound $\overline{C}$, writes:

$$\left.\frac{\partial \overline{C}}{\partial t}\right|_{convection} = -\frac{1}{\rho A}\frac{\partial (MC)}{\partial z} - \overline{w}\frac{\partial \overline{C}}{\partial z} \tag{1}$$

where A is the grid mesh area, ρ is the air density, M is the mass flux (in kg/s) and $\overline{w}$ is the environmental subsidence to compensate the upward mass flux. C is the concentration of chemical compound in the convective cells. The mass flux term of Eq. (1) is further decomposed into:

$$\frac{\partial (MC)}{\partial z} = \frac{\partial (M^u C^u)}{\partial z} + \frac{\partial (M^d C^d)}{\partial z} \tag{2}$$

where the superscripts u and d refer to the "updrafts" and to the "downdrafts" components, respectively. The different mass flux divergences are expressed as:

$$\frac{\partial}{\partial z}(M^u C^u) = \epsilon^u \overline{C} - \delta^u C^u \tag{3}$$

$$\frac{\partial}{\partial z}(M^d C^d) = \epsilon^d \overline{C} - \delta^d C^d \tag{4}$$

where ϵ and δ are the parameterized entrainment and detrainment rates, respectively. Selecting C as the concentration of nitrogen monoxide, [NO], Eqs. (3–4) are modified to include the internal LiNOx production rates :

$$\frac{\partial}{\partial z}(M^u[\mathrm{NO}]^\mathrm{u}) = \epsilon^\mathrm{u}\overline{[\mathrm{NO}]} - \delta^\mathrm{u}[\mathrm{NO}]^\mathrm{u} + (\overline{\rho}\mathrm{A})\left.\frac{\partial [\mathrm{NO}]^\mathrm{u}}{\partial \mathrm{t}}\right|_{\mathrm{LiNOx}} \tag{5}$$

$$\frac{\partial}{\partial z}(M^d[\mathrm{NO}]^{\mathrm{d}}) = \epsilon^{\mathrm{d}}\overline{[\mathrm{NO}]} - \delta^{\mathrm{d}}[\mathrm{NO}]^{\mathrm{d}} \quad (6)$$

The two terms on the right hand side of Eqs. (5 and 6) represent the subgrid scale transport of NO. Transport of NO is assumed to take place instantaneously during each model timestep. The third term is the LiNOx term to be parameterized. For this simulation, no lightning production is allowed in the downdrafts. It is worth noting that no a-priori vertical placement of LiNOx is necessary with this approach. Once produced inside the convective column, NO molecules are redistributed by upward and downward transport and detrained in the environment. The vertical placement of LiNOx is a direct consequence of the redistribution by mass fluxes inside the convective scheme. This approach is different to what has been done in several global and regional models in which the vertical placement of LiNOx was prescribed (Jourdain et al., 2001; Meijer et al., 2001; Grewe et al., 2001; Labrador et al. 2004; Park et al., 2004; Labrador et al., 2005) based on cloud-scale modelling studies (Pickering et al., 1998).

The electrical activity in the thunderstorms is related to the vertical extension of the glaciated region where ice-ice particle rebounding collisions are efficient enough to explain the charging mechanisms (Reynolds et al., 1957; Takahashi, 1978; Saunders, 1992). A growing electrical field then results from the organization of dipolar or tripolar charge structures at storm scale (Rust et al., 2002; Barthe et al., 2005). The electrical field is broken down by a partial neutralization of the electrical charges. This is realized by a repetitive triggering of intra-cloud (IC) and cloud-to-ground (CG) flashes. The flashes lead to the formation of NO in the lightning channels after dissociation of air molecules at high temperature followed by a rapid cooling. According to the statistical regression formula of Price and Rind (1992), the total lightning frequency, f_f can be grossly estimated from mean cloud morphological parameters:

$$f_f = 3.44 \times 10^{-5} {H_{ct}}^{4.9} \quad (7)$$

H_{ct} is the cloud top height of the convective cells (in km).

ACPD

6, 5197–5229, 2006

Regional lightning NO_x sources during the TROCCINOX experiment

C. Mari et al.

EGU

Price and Rind (1993) proposed the following polynomial relationship between the thickness of the icy levels (H_{fr} in km) and the IC/CG ratio, β:

$$\beta = 0.021H_{fr}^4 - 0.648H_{fr}^3 + 7.493H_{fr}^2 - 36.54H_{fr} + 63.09 \quad (8)$$

with $1 < \beta < 50$. A scaling factor $c_{pr} = 0.97241 \exp(0.048203 \times \Delta lat \Delta lon)$ is introduced by Price and Rind (1994) to adapt f_f to different mesh sizes in interval of latitude (Δlat) and longitude (Δlon) given in degree.

The combination of Eqs. (7–8), leads to the final expression of the LiNOx production rates to be inserted in Eq. (5). It can be written in condensed form :

$$\left.\frac{\partial[NO]^u}{\partial t}\right|_{LiNOx} = \frac{\beta f_f}{1+\beta} \times P(IC) + \frac{f_f}{1+\beta} \times P(CG) \quad (9)$$

where the value of the mean production rate per CG and IC namely, $P(CG)$=6.7×10^{26} of NO molecules, and $P(IC)$=6.7×10^{25} of NO molecules, of Price et al. (1997) have been retained. It is worth noting that recent studies based on airborne observations and cloud scale modeling found that intracloud flashes are likely to be as effective in producing NO as cloud-to-ground flashes (DeCaria et al., 2000; Zhang et al., 2003; Fehr et al., 2004). It is also important to note that the estimates for the lightning NOx production based on Price and Rind (1992, 1994) and Price et al. (1997) are on the high end of current estimates in the literature (Labrador et al., 2005).

The practical implementation of the LiNOx parametrization is based on critical vertical levels defined in the deep convection scheme. IC flashes are equally distributed between the cloud top and the freezing levels. The CGs are located between the -10°C's level (or the level of free sink if below) and the ground. The NO production in flashes is assumed to be proportional to air density following Goldenbaum and Dickerson (1993).

3 Experiment and meteorological situation

3.1 Experimental design

The instrumented campaign took place in February–March 2004. The investigated region was the tropical area around Bauru (22°19′S, 49°07′E) in the São Paulo state of Brazil (Fig. 1) The region is located within the zone of most intense South Atlantic convergence zone (SACZ) convection (Liebmann et al., 1999; Carvalho et al., 2004). During the austral summer, it is characterized by frequent and vigorous mesoscale convective systems sometimes associated with extreme precipitation events (Nougès-Paegle and Mo, 1997; Liebmann et al., 2001; Carvalho et al., 2002; Carvalho et al., 2004). Most thunderstorms are associated with cold front convection in a mountainous terrain, although local thunderstorms and mesoscale convective systems are also present. In the region further west of the Bauru area, the thunderstorm characteristics are associated with local conditions, fronts, and the proximity of the Bolivian high (Pinto and Pinto, 2003). The southeastern Brazil is also one of the principal region in terms of lightning activity (Pinto et al., 1996, 1999a, b) with flash densities higher than 10 flashes $km^{-2} year^{-1}$ (Pinto and Pinto, 2003; Pinto et al., 2003).

A fully instrumented research high flying aircraft (ceiling altitude of about 12 km), a Falcon 20, operated in the middle and upper troposphere. During the intense measurement campaign the aircraft operation was coordinated with detailed ground-based and space borne systems (Schumann et al., Overview paper in preparation). Observations in the boundary layer were also available from the brasilian low-level aircraft although not during the dates studied here. This study focuses on three particular flights operated by the German Falcon 20 on 3–4 March. These flights were dedicated to the study of lightning NOx with observations of both fresh and aged LiNOx emissions. Flight 09 was a morning flight from 10:00 UTC to 14:05 UTC (07:00 LT to 11:05 LT) designed to sample the background environmental conditions, before the impact of the afternoon convective activity. Flight 10 took place in the afternoon of the same day during the peak of convective activity. The aircraft operated close to the Bauru radars and sampled outflow of fresh LiNOx emissions. Flight 11 was devoted to the study of more aged airmasses with the objective to understand how the convection from the day before impacts the ozone budget over the region.

3.2 Mesoscale situation on 3–4 March

The SACZ is a northwest-southeast oriented quasi-stationary region of enhanced convection that extends southeastward from the ITCZ region anchored over the Amazon region into the South Atlantic Ocean. Each individual SACZ episode is composed of one or several midlatitude cold fronts that intrude into the subtropics and tropics, becoming stationary for a few days over southeastern Brazil (Carvalho et al., 2004; Liebmann et al., 1999). Figures 1b and 2b show the southern branch of the SACZ extending partially over the southern South Atlantic. The SACZ is characterized by high values of wet-bulb potential temperature (θ_e) at 850 hPa, representative of moist and warm air masses. The position of the associated cold front is determined by the line of strong θ_e gradient along a North-West South-East axis. At 850 hPa, dry and cold air masses are simulated behind the cold front with low θ_e values (<320 K). Between 3 March and 4 March at 18:00 UTC (15:00 LT), the high pressure system moves from the continent toward the south Atlantic, pushed northeastward by the cold front (Fig. 1). In the free troposphere, on 3 March at 12:00 UTC (09:00 LT), the Bauru area remains under the influence of northwesterly flow with continental origin. While the front moves northeastward over the ocean on 4 March, the flow turns more southeasterly but the Bauru region remains under the influence of warm and humid airmasses. North of the cold front, the simulated upper troposphere has relatively low ozone mixing ratios, ranging from 50–60 ppbv (not show) in agreement with the observed ozone mixing ratios. On contrast, the region south of the cold front is strongly impacted by the subtropical jet stream and the subsidence below the front. In the upper and mid-troposphere, higher ozone mixing ratios (>80 ppbv) are found in the model, most probably of stratospheric origin and large-scale advection associated with the jet.

3.3 Convective activity

The convective activity that occurred during the three Falcon flights is now documented using brightness temperatures (BT) at 10.7 μm observed from GOES-12 satellite at 12:00 and 21:00 UTC 3 March and 18:00 UTC 4 March (Figs. 3, 4 and 5). In addition, the synthetic BTs calculated from the simulation are also shown. Indeed, the use of the so-called model-to-satellite approach allows us a direct comparison between simulated BT with those observed from satellite (e.g. Morcrette, 1991; Chaboureau et al., 2000; Chaboureau and Bechtold, 2005). The synthetic BT are computed using the Radiative Transfer for Tiros Operational Vertical Sounder (RTTOV) version 8.2 (Saunders et al., 2005). Observed and simulated BTs are displayed on the 30-km horizontal model grid over a sub-domain of 50×50 gridpoints covering the full flight tracks.

At 12:00 UTC 3 March a deep convective cell is observed to the northwest of Bauru (point A in Fig. 3), but is missed by the simulation. Otherwise, not much convective activity and LiNOx production are found along the track of the flight 09 in the two images showing a rather good agreement between the observation and the simulation. At 21:00 UTC 3 March, convection is well-developed over all the land part of the domain in both the observation and the simulation (Fig. 4). The convective activity is clearly associated with enhanced NO convective tendencies. The thunderstorm documented during flight 10 presents characteristics of a deep convective event with BTs less than 210 K. Lightning was also observed at 16:57 UTC by the Lightning Imaging Sensor (LIS) on board the Tropical Rainfall Measuring Mission (TRMM). The general organization of the deep convective event is well-captured by the model. However, the simulated event is located a bit too far east compared to the observation. As expected, a perfect match is not attained which makes a point-to-point comparison along the track of flight 10 difficult. At 18:00 UTC 4 March, the observed convective activity and associated NO source have moved further north (Fig. 5). The simulated BTs display a similar pattern, but with more low BTs to the west than the observed ones. The track of flight 11 encounters several convective cells in both the observation and the sim-

ACPD

6, 5197–5229, 2006

ulation, but not exactly at the same locations. Overall, the simulation appears rather realistic compared to the observation, but it can miss some individual cells probed by the Falcon. This result is further shown by the time evolution of several variables over the same domain of 50×50 gridpoints (Fig. 6). The average simulated BT displays a comparable time evolution to the observed one, but with less variation from day-to-day. However, the other simulated fields present a succession of three marked diurnal cycles. The average convective available potential energy (CAPE), the total number of intracloud lightning, and the percentage of cloud tops higher than 8 km within the domain are in phase, peaking at 18:00 UTC (15:00 LT). These simulated peaks precede the observed afternoon one by about three hours, as already noted by several studies on diurnal cycle (e.g. Chaboureau and Bechtold, 2005, among many others).

4 Aircraft observations and model analysis

Flight 09 was designed to study the environmental conditions before the peak of convective activity. The model reproduces well the meteorological parameters (not shown) along the flight track. Figure 7 shows the simulated and observed O_3 and NO-NO_y chemical species along the flight track. Two simulations were performed with and without the lightning source of NO_x. Adding the LiNOx source significantly improves the simulation of NO and NO_y with higher mixing ratios at the levels of the Falcon flight (around 12 km) in agreement with the observations. The lightning emission of NO_x is thus the major source of NO_x and NO_y in this region. The impact of the LiNOx source on ozone in the upper troposphere becomes significant during the second half of the flight with an increase of ozone mixing ratio by 10–15 ppbv when the LiNOx source is triggered. During flight 09, the first maximum of NO_x mixing ratio observed by the aircraft during its ascent is well captured. According to the model and satellite images (see previous section), this maximum of NO_x originates from convection southwest of segment A-B in Fig. 3. These high NO_x mixing ratios were then advected thus corresponding to aged sources of lightning NO_x. High mixing ratios are again observed and

ACPD
6, 5197–5229, 2006

Regional lightning NO_x sources during the TROCCINOX experiment

C. Mari et al.

EGU

simulated while the aircraft was over the Sao Paolo region, before the final descent toward Gaviao Peixoto, close to Bauru. According to the model results and the satellite images there was no convective activity over the Sao Paolo area at this time (segment G-H-I in Fig. 3). A fast vertical transport of polluted air masses from the megacity is thus unlikely. Indeed, a vertical cross-sections of NO (not shown) shows that the NO uplifted or produced by lightning in the continental convection west of the domain is transported toward the Sao Paolo region and the ocean where it mixes with clean oceanic air.

The second flight (Flight 10) was dedicated to the study of the local convection in the afternoon of the same day. The aircraft remained close to the Bauru radars and sampled fresh LiNOx emissions. In Fig. 8, observed NO mixing ratios reached very high values (>15 ppbv). Although the model reproduces the two maxima of convection activity at the beginning and the end of the flight, it cannot capture the very high observed mixing ratios of NO and NO_y. The reason for this underestimation is the coarse model resolution compared to the typical spatial and duration scales of the LiNOx events. As for flight 09, the ozone mixing ratios are increased by 10 to 20 ppbv at 12 km when the LiNOx source is active.

Flight 11 took place the day after and extended the exploration area in the upper troposphere northward up to 12°S. Observed NO and NO_y mixing ratios were lower than during the previous two flights with NO mixing ratios always less than 2 ppbv (Fig. 9). During this flight, the model tends to overestimate the observed NO and NO_y mixing ratios. This overestimation of NO_x by the model can be due to (1) overestimation of convective activity and the associated LiNOx source or (2) missing heterogeneous sinks for nitrogen reservoirs like HNO_3. The formation of HNO_3 occurs through the direct reaction of NO_2 and OH. The destruction rate of HNO_3 however is relatively slow with a lifetime of approximately 20 to 30 days in the tropics. Because the photochemical rate of destruction of HNO_3 is much slower than its production rate, especially in the tropics, the cycling of NO_x through the chemical destruction of HNO_3 is slow (Brasseur et al., 1998). Since the conversion of HNO_3 to NO_2 is slow, the supposed overesti-

ACPD
6, 5197–5229, 2006

mation of HNO_3 in the upper troposphere will not produce a large increase in the NO_x concentrations.

The less efficient conversion of NO_x to HNO_3 in the upper troposphere allows the increase of NO_x due to lightning as was show by the satellite data (Zhang et al., 2000). Thus NO_x levels in the upper troposphere will be more strongly impacted by the convective activity than by recycling from HNO_3. As shown previously, the northern part of the domain was characterized by numerous convective cells, leading to an increase of lightning produced NOx. The overestimation of NO_x by the model is certainly due mostly to the vigorous convective activity simulated during flight 11 together with a memory effect of the upper troposphere to convective activity during the previous 2 days.

5 Regional lightning NO_x budget

One important aspect of the LiNOx budget is to characterize the vertical distribution of the LiNOx source and subsequent transport by the updraft and downdraft in the convective cells. In this paper, the vertical distribution of NO_x is not given a-priori but is a consequence of the initial location of IC and CG flashes, entrainment of environmental air and detrainment at different levels of the clouds (see Sect. 2). The detrainment flux represents what is really gained by the troposphere. Figure 10 shows the total regional convective fluxes, in kg(N)/s/m, calculated from the model over the whole domain of simulation. Entrainment of NO into the convective cells is very low during the three days of simulation. It is interesting to note that the production of NO inside the convective cells is significant from 4 km to 16 km altitude with maxima obtained in the 5 km to 8 km altitude range. Within this layer, the maxima of NO production by lightning increases with time. Detrainment of NO to the environment starts at 4 km altitude and peaks at 12 km on 3 March at 12:00 UTC and 14–15 km during the max of convective activity. The maximum of NO detrained to the environment is obtained during the day of maximum regional LiNOx production on 4 March at 18:00 UTC. From these profiles,

ACPD

6, 5197–5229, 2006

it is clear that the NO detrained back to the environment mainly originates from lightning source inside the convective column. Only a small fraction is pumped from the boundary layer. The production of LiNOx in kg(N)/s/m shows high values below the cloud base which are associated with the production in the CG lightnings below the cloud base and to a much lesser extent to the redistribution by downdrafts of LiNOx produced in the updrafts (no production of LiNOx is allowed in the downdrafts). There was no appropriate measurements during the studied flights to confirm or not the production of NO below the cloud base. This production however remains confined below the cloud base with very low re-entrainement into the cloud. If the regional vertical profiles of detrainment fluxes of NO are now integrated over the vertical (i.e. sum over the layer from 4 to 16 km height), the total NO production by lightning released to the troposphere ranges between 75 kg(N)/s to 400 kg(N)/s (Fig. 11). The integrated detrainment fluxes have a well pronounced diurnal cycle with peaks between 15:00 and 18:00 UTC like other convective parameters (Fig. 6). The detrainment by the downdrafts is two orders of magnitude lower than the detrainment by the updrafts (in the layer from 4 to 16 km height). The count of active convective columns in the model varies from 500 (during nighttime) to 3000 (during daytime on 4 March 2004 at 18:00 UTC) which represents about 5 to 30% of the total number of grid points in the model. This count is coherent with the percentage of observed and simulated deep convective events over the domain (Fig. 6 (middle)). The detrainment flux of NO per convective column based on the regional flux divided by the total number of active convective cells gives a production between 0.02 to 0.8 kg(N)/s/convective cell. This production per convective column is in the range of the production rates deduced from NO_x storm budgets. During the STERAO campaign, Skamarock et al. (2003) derived a production of about 0.2 kg(N)/s from the observations. A production of 0.058 kg(N)/s/anvil can be deduced from the study of Huntrieser et al. (1998) based on the flux of detrained air in the anvil and aircraft observation of NO_x mixing ratios in the anvil.

An important objective when studying particular convective episodes is to quantify the contribution of the convection and associated LiNOx source to the regional and

ACPD
6, 5197–5229, 2006

global nitrogen budget. The extrapolation method however is not straightforward. The daily regional detrainment fluxes are respectively 1.8×10^{7} kg(N)/day for 3 March 2004 and 2.5×10^{7} kg(N)/day for 4 March 2004. From Christian et al. (2003), a rough estimate of the relative lightning activity occuring over southern America can be derived. From Figs. 7 and 8 of the cited paper, it can be estimated that lightning activity over southern America in March is about 18% of the global activity. From the annual cycle of the global flash rate, it can be estimated that lightning activity in March represents about 8% of the annual global activity.

The daily production rates obtained for the 3 and 4 March 2004 are now assumed to be representative of March. It is worth noting however that these particular days were not typical average days as they were chosen for their high convective activity. This hypothesis may thus contributes to overestimate the global LiNOx production rates derived below. Assuming also that the simulated region is representative of continental southern America (90S-Eq,180W-30W), the extrapolation gives a global detrainment rate (or LiNOx production rate) between 39 to 55 Tg(N)/year. This global detrainment rate (or global LiNOx production rate) is on the high end of global LiNOx production rate estimates (Price et al., 1997; Lee et al., 1997; Huntrieser et al., 1998). This estimate is below the global production rate calculated by Skamarock et al. (2003) when multiplying the LiNOx production rate in the 10 July STERAO storm by the storm frequency number following Huntrieser et al. (1998). Uncertainties in the LiNOx source are related to the vertical placement of the IC and CG flashes, the number of flashes and associated NO molecules produced per flash, the initial and lateral boundary NOx profiles and transport parameterization. This work also represents a first attempt to deduce a global scale LiNOx budget from a regional scale simulation. Further work is needed to reduce the uncertainties, to reconciliate the different approaches and provide a proper way to extrapolate storm and regional NO_x budget to global scale.

6 Conclusions

A lightning NO_x source has been implemented in the deep convection scheme of the Meso-NH mesoscale model. The LiNOx scheme is written following a mass-flux formalism coherent with the transport and scavenging of gases inside the convective scheme. No a-priori vertical placement of LiNOx is necessary with this approach. Once produced inside the convective column, NO molecules are redistributed by updrafts and downdrafts and detrained in the environment when the conditions are favorable. The model was applied to three particular flights during the TROCCINOX campaign over the tropical area around Bauru on 3–4 March 2004. These flights operated by aircraft measurements were dedicated to the study of lightning NO_x with observations of both fresh and aged LiNOx emissions. The convective activity during the three flights was investigated using brightness temperature at 10.7 μm observed from GOES-12 satellite. The use of a model-to-satellite approach reveals that the simulation appears rather realistic compared to the observations. The model can miss some individual cells sampled by the aircraft due to the low horizontal resolution of the model compared to the scale of the cells. The diurnal cycle of the simulated brightness temperature, CAPE, number of IC lightning, NO entrainment flux are in phase, with a succession of three marked peaks at 18:00 UTC (15:00 LT). These simulated peaks precede the observed afternoon one by about three hours, as already noted by several studies on diurnal cycle. Comparison of the simulated NO_x with observations along the flight tracks show that the model reproduces well the observed NO_x levels when the LiNOx source is applied. Exceptions are the very high levels of NO_x observed in the anvils during flight 10 and which horizontal and temporal resolutions are much higher than the model ones. The model tends to overestimate the NO_x levels in the upper troposphere during the last flight which can be due to high convective activity in the model. The budget of entrainment, detrainment and LiNOx convective fluxes shows that the majority of the NO detrained back to the environment comes from lightning source inside the convective columns. Entrainment of NO from the environment and vertical transport from the

ACPD
6, 5197–5229, 2006

Regional lightning NO_x sources during the TROCCINOX experiment

C. Mari et al.

EGU

boundary layer were not significant during the episode. The troposphere is impacted by detrainment fluxes of LiNOx from 4 km altitude to 16 km with maximum values around 14 km altitude. Detrainment fluxes vary between 75 kg(N)/s during nighttime to 400 kg(N)/s at the times of maximum convective activity. A first extrapolation of these regional fluxes gives global LiNOx production between 39–55 Tg(N)/year which is above the upper range of current estimates. Further work is still needed to reconciliate the global, regional and storm approaches and provide a way to extrapolate case studies to global NO_x budget.

Acknowledgements. Computer time has been provided by the Institute du Développement et des Ressources en Informatique Scientifique (IDRIS). We thanks V.-H. Peuch from Meteo-France/CNRM/GAME for providing us with the large-scale chemistry fields from the MOCAGE CTM model. This research was supported by the TROCCINOX project funded by the European Comission under the contract EVK2-CT-2001-00122.

References

Barthe, C., G. Molinio, and J.-P. Pinty: Description and first results of an explicit electrical scheme in a 3D cloud resolving model, Atmospheric Research, 76, 95–113, 2005.

Bechtold P., E. Bazile, F. Guichard, P. Mascart and E. Richard: A mass-flux convection scheme for regional and global models, Q.J.R. Meteorol. Soc., 127, 869–886, 2001.

Bradshaw, J., Davis, D., Grodzinsky, G., Smyth, S., Newell, R., Sandholm, S., and Liu, S.: Observed distributions of nitrogen oxides in the remote free troposphere from the NASA global tropospheric experiment programs, Rev. of Geophysics, 38, 61–116, 2000.

Brasseur, G., Muller, J. F., and Granier, C.: Atmospheric impact of NO_x emissions by subsonic aircraft: A three-dimensional model study, J. Geophys. Res., 101, 1423–1428, 1996.

Brasseur G., Hauglustaine, D. A., Walters, S., Rasch, P. J., Muller, J.-F., Granier, C., and Tie, X. X.: MOZART, a global chemical transport model for ozone and related chemical tracers, 1, Model description, J. Geophys. Res., 103, 28 265–28 289, 1998.

Brunner D., Staehelin, J., Rogers, H. L., Kohler, M. O., Pyle, J. A., Hauglustaine, D., Jourdain, L., Berntsen, T. K., Gauss, M., Isaksen, I., Meijer, E., van Velthoven, P., Pitari, G., Mancini, E., Grewe, V., and Sausen, R.: An evaluation of the performance of chemistry transport models by comparison with research aircraft observations, Part 1: concepts and overall model performance, Atmos. Chem. Phys., 3, 1609–1631, 2003.

Carvalho, L. M., Jones, C., and Liebmann, B.: Extreme precipitation events in southeastern South America and large-scale convective patterns in the South Atlantic Convergence Zone, J. Clim., 15, 2377–2394, 2002.

Carvalho, L. M., Jones, C., Liebmann, B.: The South Atlantic Convergence Zone: Intensity, Form, Persistence and Relationships with Intraseasonal to Interannual activity and extreme rainfall, J. Clim., 17, 88–108, 2004.

Chaboureau, J.-P. and Bechtold, P.: Statistical representation of clouds in a regional model, and the impact on the diurnal cycle of convection during TROCCINOX J. Geophys. Res., doi:10.1029/2004JD005645, 2005.

Chaboureau, J.-P., Cammas, J.-P., Mascart, P., Pinty, J.-P., Claud, C., Roca, R., and Morcrette, J. J.: Evaluation of a cloud system life-cycle simulated by Meso-NH during FASTEX using METEOSAT radiances and TOVS-3I cloud retrievals, Quart. J. Roy. Meteor. Soc., 126, 1735–1750, 2000.

Christian, H. J., Blakeslee, R. J., Boccippio, D. J., Boeck, W. L., Buechler, D. E., Driscoll, K. T., Goodman, S. J., Hall, J. M., Koshak, W. J., Mach, D. M., and Stewart, M. F.: Global frequency and distribution of lightning as observed from space by the Optical Transient Detector, J. Geophys. Res., Art No. 4005, 2003.

Crassier, V., Suhre, K., Tulet, P., and Rosset, R.: Development of a reduced chemical scheme for use in mesoscale meteorological models, Atm. Env., 34, 2633–2644, 2000.

Crawford, J., Davis, D., Olson, J., et al.: Evolution and chemical consequences of lightning-produced NO_x observed in the North Atlantic upper troposphere, J. Geophys. Res., 105, 19 795–19 809, 2000.

DeCaria, A. J., Pickering, K. E., Stenchikov, G. L., et al.: A cloud-scale model study of lightning-generated NO_x in an individual thunderstorm during STERAO-A, J. Geophys. Res., 105, 11 601–11 616, 2000.

DeCaria, A. J., Pickering, K. E., Stenchikov, G. L., and Ott, L. E.: Lightning-generated NO_x and its impact on tropospheric ozone production: A three-dimensional modeling study of a Stratosphere-Troposphere Experiment: Radiation, Aerosols and Ozone (STERAO-A) thunderstorm, J. Geophys. Res., 110, Art. No. D14303, 2005.

Dye, J. E., Ridey, B. A., Skamarock, W. et al.: An overview of the Stratospheric-Tropospheric Experiment: Radiation, Aerosols, and Ozone (STERAO)-Deep Convection experiment with

results for the 10 July 1996 storm, J. Geophys. Res., 105, 10 023–10 045, 2000.
Fehr, T., Holler, H., and Huntrieser H.: Model study on production and transport of lightning-produced NO_x in a EULINOX supercell storm J. Geophys. Res., 109, Art. No. D09102, 2004.
Goldembaum, G. C. and Dickerson, R. R.: Nitric oxide production by lightning discharges, J. Geophys. Res, 98, 18 333–18 338, 1993.
Grewe, V., Brunner, D., Dameris, M., Grenfell, J. L., Hein, R., Shindell, D., and Staehelin, J.: Origin and variability of upper tropospheric nitrogen oxides and ozone at northern mid-latitudes, Atm. Env., 35, 3421–3433, 2001.
Hauglustaine, D., Emmons, L., Newchurch, M., et al.: On the role of lightning NO_x in the formation of tropospheric ozone plumes: A global model perspective, J. Atm. Chem., 38, 277–294, 2001.
Huntrieser, H., Schlager, H., Feigl, C., et al.: Transport and production of NO_x in electrified thunderstorms: Survey of previous studies and new observations at midlatitudes J. Geophys. Res., 103, 28 247–28 264, 1998.
Huntrieser, H., Feigl, C., Schlager, H., Schroder, F., Gerbig, C., van Velthoven, P., Flatoy, F., Thery, C., Petzold, A., Holler, H., and Schumann, U.: Airborne measurements of NO_x, tracer species and small particles during the European Lightning Nitrogen Oxides Experiment J. Geophys. Res., 107, Art. No. 4113, 2002.
Josse, B., Simon, P., Peuch, V. H., Radon global simulations with the multiscale chemistry and transport model MOCAGE, Tellus Ser. B, 56, 339–356, 2004.
Jourdain, L. and Hauglustaine, D. A.: The global distribution of lightning NO_x simulated on-line in a general circulation model, Physics and Chemistry of the Earth, 26, 585–591, 2001.
Labrador, L. J., von Kuhlmann, R., and Lawrence, M. G.: Strong sensitivity of the global mean OH concentration and the tropospheric oxidizing efficiency to the source of NO_x from lightning Geophys. Res. Let., 31, Art. No. L06102, 2004.
Labrador, L. J., von Kuhlmann, R., and Lawrence, M. G.: The effects of lightning-produced NO_x and its vertical distribution on atmospheric chemistry: sensitivity simulations with MATCH-MPIC Atmos. Chem. Phys., 5, 1815–1834, 2005.
Lafore, J. P., Stein, J., Asencio, N., et al.: The Meso-NH Atmospheric simulation system, I. Adiabatic formulation and control simulations, Ann. Geophys., 16, 90–109, 1994.
Lamarque, J.-F., Brasseur, G., Hess, P., and Muller, J.-F.: Three-dimensional study of the reactive contributions of the different nitrogen sources in the troposphere, J. Geophys. Res., 102, 10 873–10 873, 1997.

Lee, D. S., Köhler, I., Grobler, E., Rohrer, F., Sausen, R., Gallardo-Klenner, L., Olivier, J. G. L., Dentener, F. J., and Bouwman, A. F.: Estimations of Global NOx emissions and their uncertainties, Atm. Env., 31, 1735–1749, 1997.

Liebmann, B., Kiladis, G. N., Marengo, J. A., Ambrizzi, T., and Glick, J. D.: Submonthly convective variability over the South America and the South Atlantic convergence zone, J. Clim., 12, 1877–1891, 1999.

Liebmann, B., Jones, C., and de Carvalho, L. M. V.: Interannual variability of daily extreme precipitation events in the state of São Paulo, Brazil, J. Clim., 14, 208–218, 2001.

Mari, C., Jacob, D. J., and Bechtold, P.: Transport and scavenging of soluble gases in a deep convective cloud, J. Geophys. Res, 105, 22 255–22 267, 2000.

Martin, R. V., Jacob, D. J., Logan, J., Ziemke, J. M., and Washington, R.: Detection of a lightning influence on tropical tropospheric ozone, Geophys. Res. Let., 27, 1639–1642, 2000.

Massart, S., Cariolle, D., and Peuch, V. H.: Towards an improvement of the atmospheric ozone distribution and variability by assimilation of satellite data, Comptes Rendus Geoscience, 337, 1305–1310, 2005.

Masson, V.: A physically-based scheme for the urban energy budget in atmospheric models. Bound. Layer Meteor, 1994, 357–397, 2000.

Meijer, E. W., van Velthoven, P. F. L., Brunner, D., Huntrieser, H., and Kelder, H.: Improvement and evaluation of the parameterisation of nitrogen oxide production by lightning, Phys. Chem. Earth., 26, 577–583, 2001.

Mlawer, E. J., Taubman, S. J., Brown, P. D., Iacono, M. J., and CLough, S. A.: Radiative transfer for inhomogeneous atmospheres: RRTM, a validated correlated-k model for the longwave, J. Geophys. Res., 102D, 16 663–16 682, 1997.

Morcrette, J.-J.: Radiation and cloud radiative properties in the European centre for medium range weather forecasts forecasting system, J. Geophys. Res., 96, 9121–9132, 1991.

Noilhan, J.: A simple parameterization of land surface processes for meteorological models, Monthly Weather Rev, 117, 536, 1989.

Nougés-Paegle, J. and Mo, K. C.: Alternating wet and dry conditions over South America during summer, Mon. Wea. Rev., 125, 279–291, 1997.

Olivier, J. G. J. and Berdowski, J. J. M.: Global emissions sources and sinks. in: The Climate System, edited by: Berdowski, J., Guicherit, R., and Heij, B. J., A.A. Balkema Publishers/Swets and Zeitlinger Publishers, Lisse, The Netherlands, 33–78, 2001a.

Olivier, J. G. J., Berdowski, J. J. M., Peters, J. A. H. W., Bakker, J., Visschedijk, A. J. H., and

Bloos, J.-P. J.: Applications of EDGAR. Including a description of EDGAR 3.0: reference database with trend data for 1970–1995, RIVM, Bilthoven. RIVM report no. 773301 001/ NOP report no. 410200 051, 2001b.

Park, M., Randel, W. J., Kinnison, D. E., Garcia, R. R., and Choi, W.: Seasonal variation of methane, water vapor, and nitrogen oxides near the tropopause: Satellite observations and model simulations, J. Geophys. Res., 109, Art. No. D03302, 2004.

Pickering, K. E., Wang, Y. S., Tao, W. K., Price, C., and Muller, J. F.: Vertical distributions of lightning NO_x for use in regional and global chemical transport models, J. Geophys. Res., 103, 31 203–31 216, 1998.

Pinto O., Gin, R. B. B., Pinto, I. R. C. A., Mendes, O., Diniz, J. H., and Carvalho, A. M.: Cloud-to-ground lightning flash characteristics in southeastern Brazil for the 1992–1993 summer season, J. Geophys. Res., 101, 29 627–29 635, 1996.

Pinto, O., Pinto, I. R. C. A., Gomes, M. A. S. S., Vitorello, I., Padilha, A. L., Diniz, J. H., Carvalho, A. M., and Cazetta Filho, A.: Cloud-to-ground lightning in southeastern Brazil in 1993 1. Geographical distribution, J. Geophys. Res., 104, 31 369–3 1379, 1999a.

Pinto, I. R. C. A., Pinto, O., Rocha, R. M. L., Diniz, J. H., Carvalho, A. M., and Cazetta Filho, A.: Cloud-to-ground lightning in southeastern Brazil in 1993: 2. Time variations and flash characteristics, J. Geophys. Res., 104, 31 381–31 387, 1999b.

Pinto, I. R. C. A. and Pinto, O.: Cloud-to-ground lightning distribution in Brazil, J. Atm. Solar-Terr. Phys., 65, 733–737, 2003.

Pinto, O., Pinto, I. R. C. A., Diniz, J. H., Fihlo, A. C., Cherchiglia, L. C. L., and Carvalho, A. M.: A seven-year study about the negative cloud-to-ground lightning flash characteristics in Southeastern Brazil, J. Atm. Solar-Terr. Phys., 65, 739–748, 2003.

Price, C. and Rind, D.: A simple lightning parameterization for calculating global lightning distributions, J. Geophy. Res., 97, 9919–9933, 1992.

Price, C. and Rind, D.: What determines the cloud-to-ground lightning fraction in thunderstorms?, Geophys. Res. Lett., 20, 463–466, 1993.

Price, C. and Rind, D.: Modeling global lightning distributions in a General Circulation Model, Mon. Wea. Rev., 122, 1930–1939, 1994.

Price, C., Penner, J., and Prather, M.: NO_x From Lightning, Part I: Global Distribution Based on Lightning Physics, J. Geophys. Res., 102, 5929–5941, 1997.

Reynolds, S. E., Brooks, M., and Gourley, M. F.: Thunderstorm charge separation, J. Meteor., 14, 426–436, 1957.

Rust W. D. and MacGorman, D. R.: Possibly inverted-polarity electrical structures in thunderstorms during STEPS, Geophys. Res. Lett., 29, doi:10.1029/2001GL014303, 2002.
Saunders, C. P. R.: A review of thunderstorm electrification processes, J. Appl. Meteor., 32, 642–655, 1992.
Saunders, R., Brunel, P., English, S., Bauer, P., O'Keeffe, J., Francis, P., and Rayer, R.: RTTOV-8 Science and validation report. NWP SAF Report, 41 pp., 2005.
Skamarock, W. C., Powers, J., Barth, M. C., Dye, J., Matejka, T., Bartels, D., Baumann, K., Stith, J. L., Parrish, D., and Hubler, G.: Numerical simulations of the 10 July STERAO/Deep convection experiment convective system: Kinematics and transport, J. Geophys. Res., 105, 19 973–19 990, 2000.
Skamarock, W. C., Dye, J. E., Defer, E., Barth, M. C., Stith, J. L., Ridley, B. A., and Baumann, K.: Observational- and modeling-based budget of lightning-produced NO_x in a continental thunderstorm, J. Geophys. Res., 108, Art. No. 4305, 2003.
Takahashi, T.: Riming electrification as a charge generation mechanism in thunderstorms, J. Atmos. Sci., 35, 1536–1548, 1978.
Tie, X. X., Zhang, R. Y., Brasseur, G., Emmons, L., and Lei, W.: Effects of lightning on reactive nitrogen and nitrogen reservoir species in the troposphere, J. Geophys. Res., 106, 3167–3178, 2001.
Zhang, R., Sanger, N. t., Orville, R. E., Tie, X. X., Randel, W., and Williams, E. R.: Enhanced NO_x by lightning in the upper troposphere and lower stratosphere inferred from the UARS global NO_2 measurements, Geophys. Res. Let., 27, 685–688, 2000.
Zhang, X. J., Helsdon, J. H., and Farley, R. D.: Numerical modeling of lightning-produced NO_x using an explicit lightning scheme: 1. Two-dimensional simulation as a "proof of concept", J. Geophys. Res., 108, A1–A20, 2003.

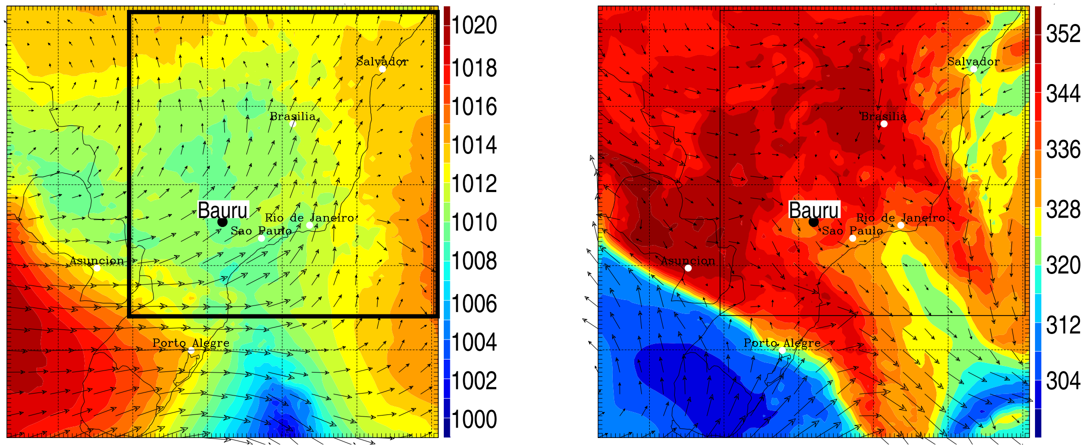

(a) (b)

Fig. 1. Simulated meteorology on 3 March at 12:00 UTC (09:00 LT): **(a)** mean sea level pressure in hPa and wind vectors at the surface, **(b)** wet-bulb potential temperature in K and wind vectors at 850 hPa. The inside domain is used for Figs. 3, 4 and 5.

ACPD

6, 5197–5229, 2006

Regional lightning NO_x sources during the TROCCINOX experiment

C. Mari et al.

EGU

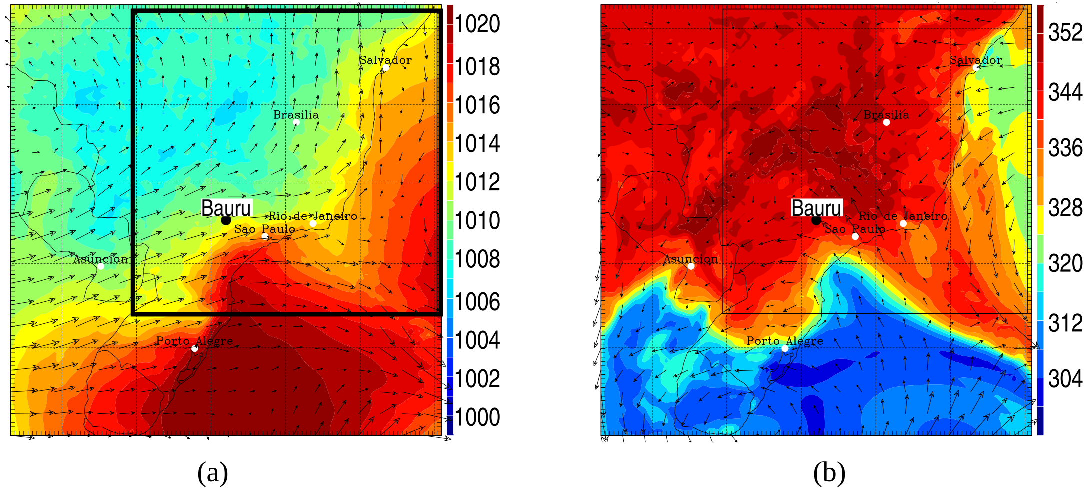

Fig. 2. Same as Fig. 1 on 4 March at 18:00 UTC (15:00 LT).

ACPD

6, 5197–5229, 2006

Regional lightning NO_x sources during the TROCCINOX experiment

C. Mari et al.

EGU

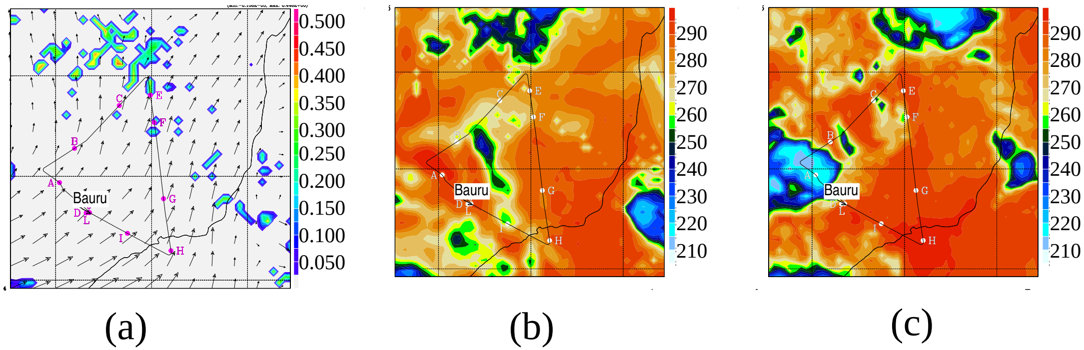

Fig. 3. **(a)** Simulated convective tendency for NO in pptv/s at 12 km, **(b)** 10.7 μm BTs (K) obtained from the Meso-NH simulation and **(c)** 10.7 μm BTs (K) obtained from GOES-12 observation on 3 March 2004 at 12:00 UTC. Black line displays the track of flight 9.

ACPD
6, 5197–5229, 2006

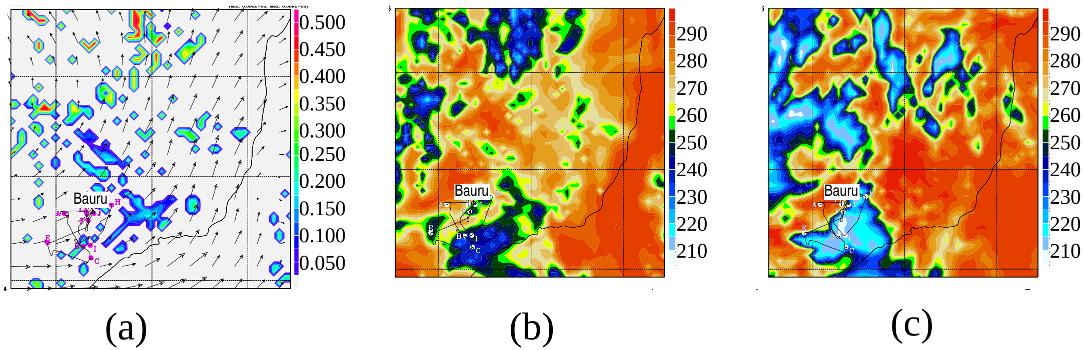

Fig. 4. Same as Fig. 3 for flight 10 on 3 March at 21:00 UTC.

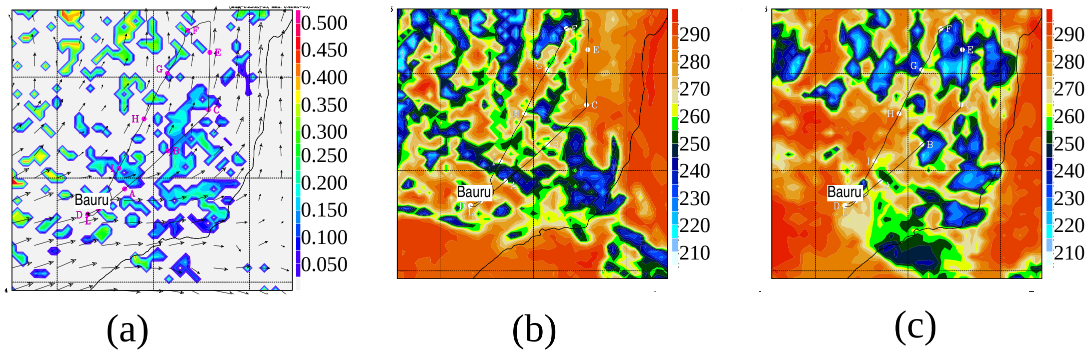

Fig. 5. Same as Fig. 3 for flight 11 on 4 March at 18:00 UTC.

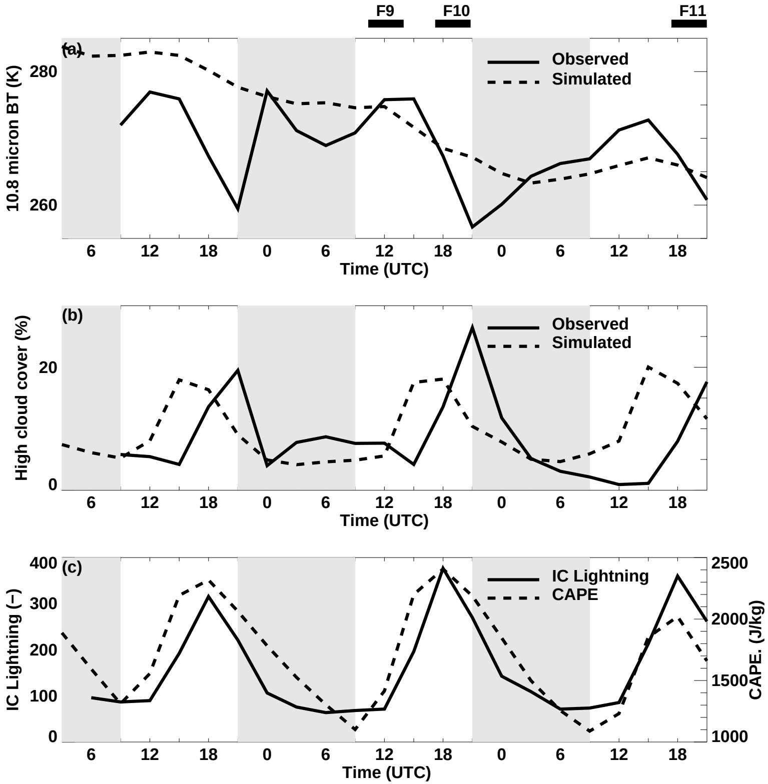

Fig. 6. Time evolution of several convective fields from 03:00 UTC 2 March till 21:00 UTC 4 March over the domain shown in Fig. 3. Grey shading indicate night periods. (top) Observed and simulated 10.7 μm averaged BTs (K). (middle) Percentage of observed and simulated high cloud cover over the domain (%). (bottom) Total number of simulated intracloud ligthning and averaged convective available potential energy (Jkg^{-1}).

ACPD
6, 5197–5229, 2006

Title Page
Abstract | Introduction
Conclusions | References
Tables | Figures
◀| |▶
◀ ▶
Back | Close
Full Screen / Esc
Printer-friendly Version
Interactive Discussion

EGU

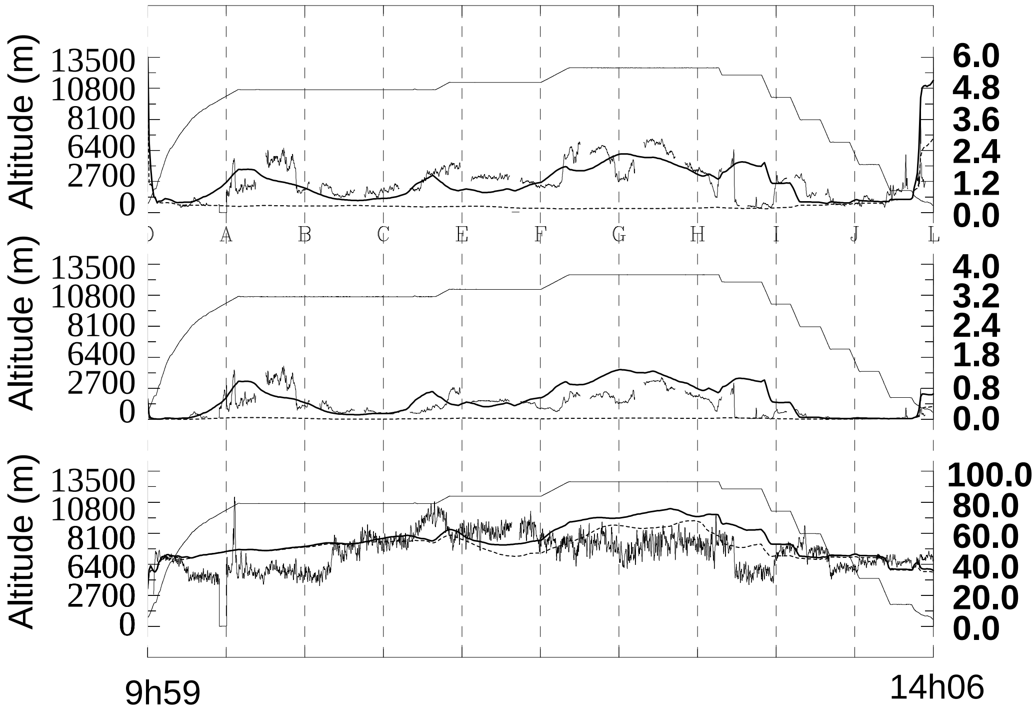

Fig. 7. Simulated and observed (thick solid line) values over the entire duration of flight 09 of **(a)** NO_y in ppbv, **(b)** NO in ppbv and **(c)** O_3 in ppbv. The thin solid line represents the altitude of the flight in hPa. The dotted lines represents the mixing ratios without the LiNOx source (close to zero for NO and NO_y).

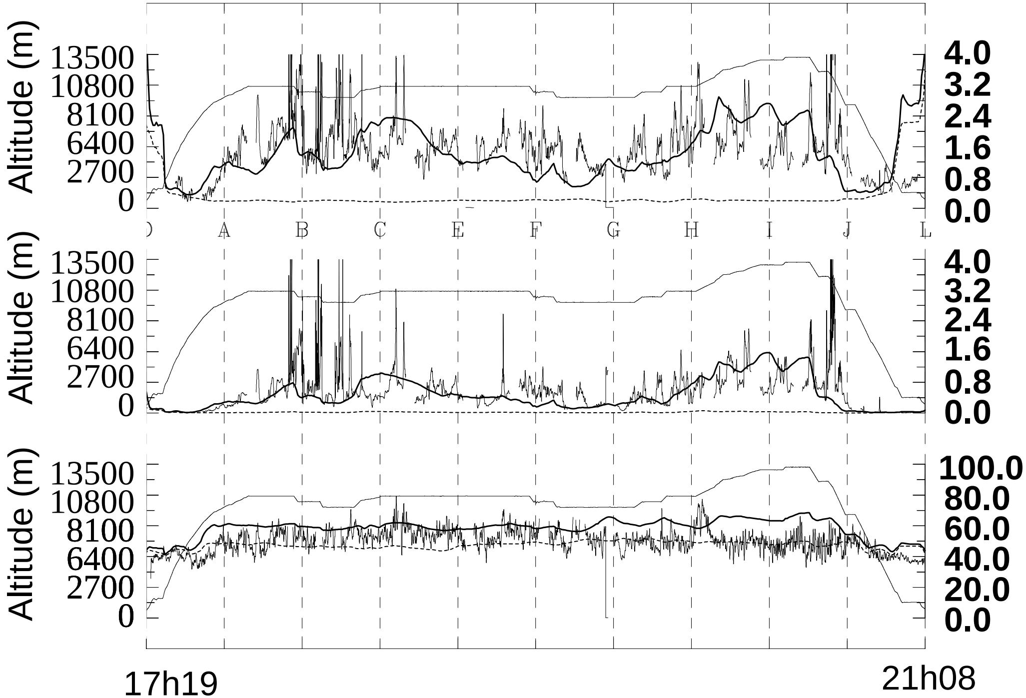

Fig. 8. Same as Fig. 7 for flight 10.

ACPD

6, 5197–5229, 2006

Regional lightning NO_x sources during the TROCCINOX experiment

C. Mari et al.

EGU

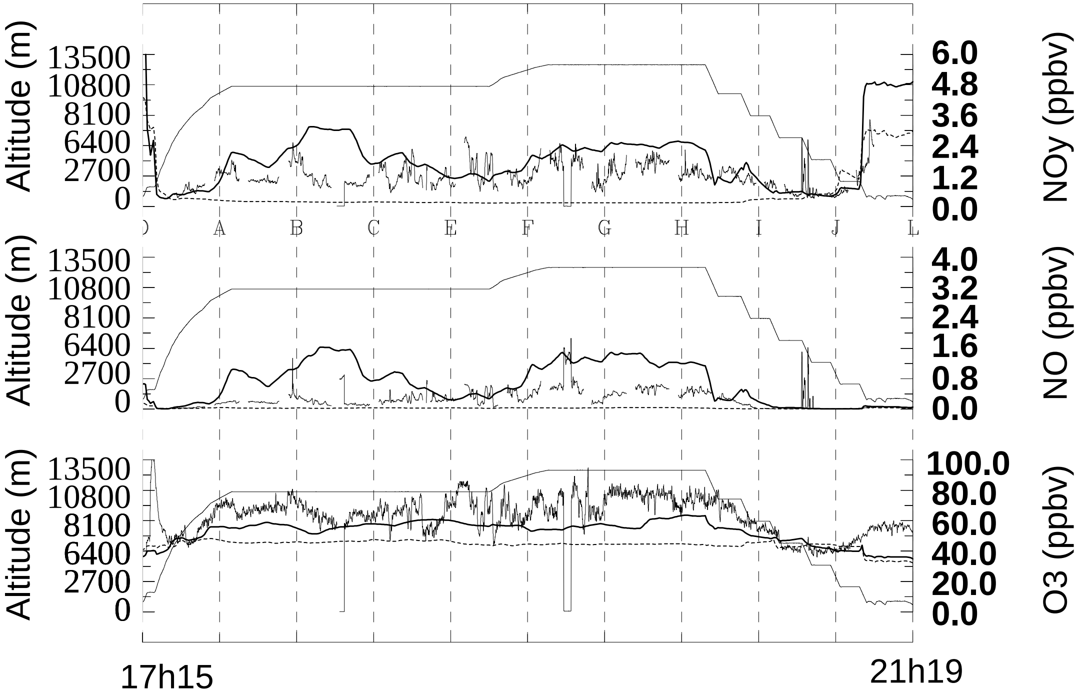

Fig. 9. Same as Fig. 7 for flight 11.

ACPD
6, 5197–5229, 2006

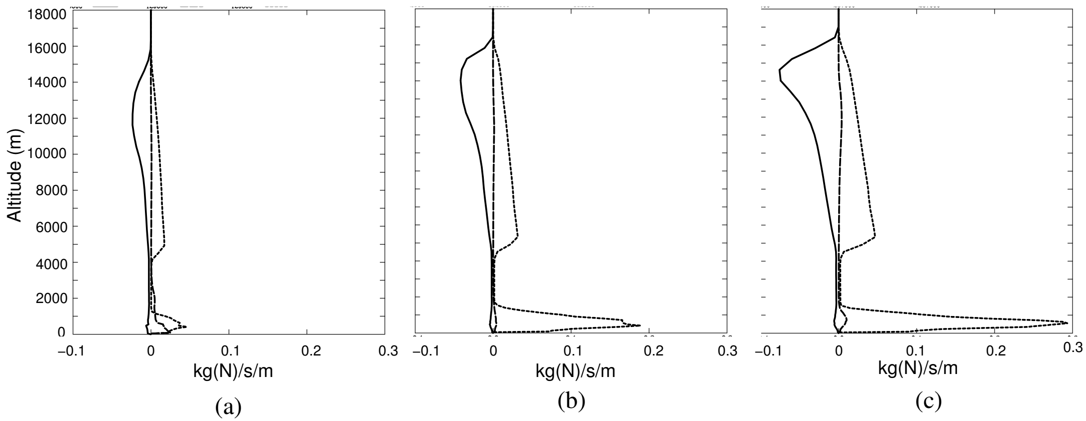

Fig. 10. Total simulated vertical profiles of convective detrainment flux (solid line), entrainment fluxes (dashed line) and lightning NO production flux (dotted line), in kg(N)/s/m at **(a)** 12:00 UTC (09:00 LT) on 3 March, **(b)** 21:00 UTC (18:00 LT) on 3 March 2004 and **(c)** 18:00 UTC (15:00 LT) on 4 March 2004. The fluxes are summed over the whole domain of simulation (see Fig. 1).

ACPD
6, 5197–5229, 2006

Regional lightning NO_x sources during the TROCCINOX experiment

C. Mari et al.

Title Page
Abstract Introduction
Conclusions References
Tables Figures
◀I ▶I
◀ ▶
Back Close
Full Screen / Esc
Printer-friendly Version
Interactive Discussion

EGU

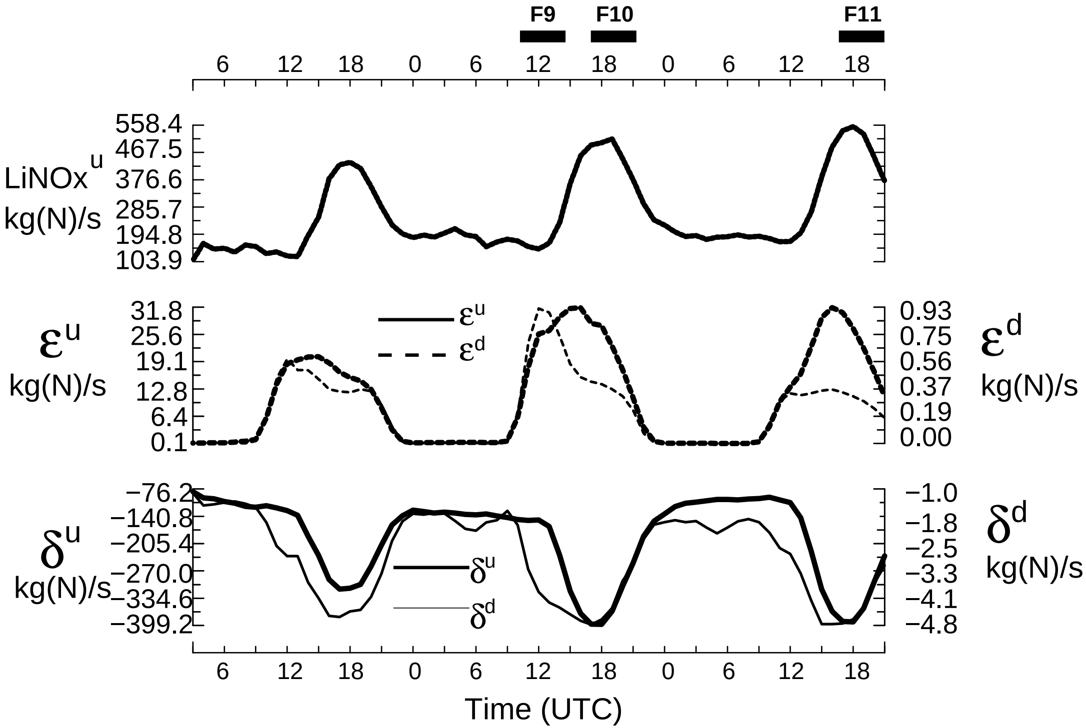

Fig. 11. Time evolution of simulated convective fluxes from 03:00 UTC 2 March till 21:00 UTC 4 March summed over the domain shown in Fig. 3, for the layer from 4 to 16 km height, in kg(N)/s. (top) NO production by lightning in the updrafts ($(\overline{\rho}A)\frac{\partial[NO]^u}{\partial t}\Big|_{LiNOx}$) (middle) entrainment fluxes in the updrafts $\epsilon^u\overline{[NO]}$ (thick dashed line) and the downdrafts $\epsilon^d\overline{[NO]}$ (thin dashed line) (bottom) detrainment fluxes in the updrafts $-\delta^u[NO]^u$ (thick solid line) and the downdrafts $-\delta^d[NO]^u$ (thin solid line).

ACPD
6, 5197–5229, 2006

Regional lightning NO_x sources during the TROCCINOX experiment

C. Mari et al.

EGU